Phosphoregulation of an Inner Dynein Arm Complex in *Chlamydomonas reinhardtii* Is Altered in Phototactic Mutant Strains

Stephen J. King and Susan K. Dutcher

Department of Molecular, Cellular, and Developmental Biology, University of Colorado at Boulder, Boulder, Colorado 80309-0347

Abstract. To gain a further understanding of axonemal dynein regulation, mutant strains of *Chlamydomonas reinhardtii* that had defects in both phototactic behavior and flagellar motility were identified and characterized. *ptm*1, *ptm*2, and *ptm*3 mutant strains exhibited motility phenotypes that resembled those of known inner dynein arm region mutant strains, but did not have biochemical or genetic phenotypes characteristic of other inner dynein arm mutations. Three other mutant strains had defects in the *f* class of inner dynein arms. Dynein extracts from the *pf*9-4 strain were missing the entire *f* complex. Strains with mutations in *pf*9/*ida*1, *ida*2, or *ida*3 failed to assemble the *f* dynein complex and did not exhibit phototactic behavior. Fractionated dynein from *mia*1-1 and *mia*2-1 axonemes exhibited a novel *f* class inner dynein arm biochemical phenotype; the 138-kD *f* intermediate chain was present in altered phosphorylation forms. In vitro axonemal dynein activity was reduced by the *mia*1-1 and *mia*2-1 mutations. The addition of kinase inhibitor restored axonemal dynein activity concomitant with the dephosphorylation of the 138-kD *f* intermediate chain. Dynein extracts from *uni*1-1 axonemes, which specifically assemble only one of the two flagella, contained relatively high levels of the altered phosphorylation forms of the 138-kD intermediate chain. We suggest that the *f* dynein complex may be phosphoregulated asymmetrically between the two flagella to achieve phototactic turning.

Chlamydomonas reinhardtii flagella use an asymmetric beat stroke, similar to a breast stroke, to propel cells forward. To generate the asymmetric beat stroke, dynein activity must be regulated both along the length and around the circumference of the flagella. If all dyneins were active at the same time, the flagella would exist in a state of rigor. The dyneins are located in two rows along the length of the doublet microtubules. The inner dynein arms are heterogeneous in composition with at least eight heavy chains and various intermediate and light chains arranged in an elaborate morphology that repeats every 96 nm (Kagami and Kamiya, 1992; Mastronarde et al., 1992). In contrast, the outer dynein arms are biochemically and morphologically homogeneous (Huang et al., 1979; Mitchell and Rosenbaum, 1985; Kamiya, 1988); each outer dynein arm contains three dynein heavy chains and 10 intermediate and light chains. The inner and outer arms appear to have different functions in the formation of the beat stroke; the inner arms generate the waveform of the beat stroke, whereas the outer arms provide additional force to the waveform (Brokaw and Kamiya, 1987).

Previous workers had shown that dynein regulation is imposed, in part, by activities of the radial spokes and the central pair complex. Mutant strains that are missing or have altered radial spokes or central pair complexes are paralyzed even if they have a full complement of dyneins (Adams et al., 1981; Piperno et al., 1981). Many extragenic suppressors of this paralysis phenotype do not restore the missing structures, but rather suppress by altering either inner arm or outer arm region structures (Huang et al., 1982*a*; Piperno et al., 1992; Porter et al., 1992, 1994). These data suggest that direct or indirect interactions exist between the dynein arms and the radial spokes or central pair complexes.

Over 80 proteins in *Chlamydomonas* flagella are phosphorylated (Piperno et al., 1981), which makes dynein regulation by phosphorylation an attractive model. Hasegawa et al. (1987) showed that a higher percentage of demembranated axonemes reactivate with ATP after treatments that lower cAMP levels or inhibit cAMP-dependent protein kinase (cAPK)[1]. In flagella from other organisms, cAMP has an opposite role (for reviews see Tash and Means, 1983; Tash, 1989). An increased frequency of reac-

Address all correspondence to Susan K. Dutcher, Department of Molecular, Cellular, and Developmental Biology, University of Colorado at Boulder, Boulder, CO 80309-0347. Tel.: (303) 492-6748. Fax: (303) 492-7744.

S.J. King's present address is Department of Biology, 204 Mudd Hall, The Johns Hopkins University, Baltimore, MD 21218.

1. *Abbreviations used in this paper*: cAPK, cAMP-dependent protein kinase; CIP, calf intestinal phosphatase; drc, dynein regulatory complex; HA-1004, *N*-(2-guanidinoethyl)-5-isoquinolinesulfonamide hydrochloride.

tivation also occurs after the NP-40–soluble components are extracted from the axonemes, which suggests that the cAPK, target phosphoproteins, and endogenous phosphatases are all integral axonemal components (Hasegawa et al., 1987). In quantitative sliding disintegration assays, the inner dynein arm activity of axonemes that are missing the radial spokes is increased in the presence of pharmacological or specific peptide inhibitors of cAPK (Smith and Sale, 1992; Howard et al., 1994). Reconstitution experiments with axonemes that are missing the radial spokes suggest that radial spokes normally function to activate the inner dynein arms by inhibiting a cAPK (Smith and Sale, 1992; Howard et al., 1994). It is not known if the cAPK directly phosphorylates inner dynein arm components or phosphorylates another axonemal component that then acts on the inner dynein arms (Howard et al., 1994).

The *f* (originally called I1) inner arms are biochemically the best studied inner dynein arm complex. This complex is comprised of two dynein heavy chains and three intermediate chains of 140, 138, and 110 kD; it can be purified by sucrose density centrifugation (Piperno and Luck, 1981; Smith and Sale, 1991; Porter et al., 1992) or ion-exchange chromatography (Kagami and Kamiya, 1992). The purified complex has low ATPase activity and only rarely translocates microtubules in vitro (Smith and Sale, 1991; Kagami and Kamiya, 1992). Deep-etch EM of the purified *f* inner arm shows a two-headed complex that is connected to a common base by thin stalks (Smith and Sale, 1991). Longitudinal EM image analyses have shown that this complex is located just proximally of the first radial spoke in each 96-nm repeating unit (Piperno et al., 1990; Mastronarde et al., 1992). Mutations at three different loci (*PF*9/*IDA*1, *IDA*2, and *IDA*3) result in the complete loss of the *f* complex (Kamiya et al., 1991; Kagami and Kamiya, 1992; Porter et al., 1992). The *PF*9/*IDA*1 locus encodes a dynein heavy chain that is believed to be one of the two heavy chains that are components of the *f* complex (Porter, 1996).

We undertook a new approach to identify axonemal components involved in dynein regulation; we isolated and characterized mutant strains that were unable to perform phototaxis. In *Chlamydomonas*, phototaxis is a behavior by which cells orient to the direction of incident light. Light direction is detected by the eyespot, an asymmetrically located organelle, and a signal is transmitted to the flagella using voltage-gated ion channels (Harz and Hegemann, 1991). For cells to perform phototaxis, the waveforms of the two flagella are altered coordinately. The *trans* flagellum, which is located farther from the eyespot, beats with a larger front amplitude than the *cis* flagellum to turn the cell toward the light (Rüffer and Nultsch, 1991). It seemed likely that the alterations in the beat amplitudes needed for correct phototactic behavior could be caused by differential dynein regulation in the *cis* and *trans* flagella. Therefore, we hypothesized that there should be a class of phototactic mutant strains that is not able to perform phototaxis because of defects in the regulation of dyneins. Three of the eight phototactic mutant strains that we characterized had biochemical defects in the *f* class of inner dynein arms. One of these strains, *pf*9-4, was missing the entire *f* complex, and the other two strains, *mia*1-1 and *mia*2-1, exhibited a novel *f* class inner dynein arm biochemical phenotype. These observations suggest that the *f* inner dynein arm is a target for regulation during phototaxis.

Materials and Methods

Phototaxis Assay

Chlamydomonas reinhardtii strains were examined for their ability to perform positive phototaxis, which is the orientation of swimming cells toward a light source. Cells in liquid medium were placed inside a box with a slit along the bottom that allowed light to reach only the bottom one-third of the medium. The cells were exposed for 30 min to a 15-W fluorescent light placed 50 cm from the slit. Strains that could perform phototaxis were typically concentrated in the lighted portion of the assay tube compared with the darkened portion. Strains unable to perform phototaxis were found equally dispersed in the lighted and darkened portions of the tube.

Mutagenesis

Two mutagenesis schemes were used to generate strains of *Chlamydomonas* that could not perform phototaxis. In the first scheme, independent colonies of a wild-type strain (CC-125) were mutagenized by UV irradiation (Dutcher et al., 1988) and transferred to liquid medium. Once flagellar regrowth had occurred, the cells were subjected to a phototaxis assay. Swimming cells tend to accumulate at the surface of liquid medium. To enrich for swimming cells that were not phototactic, the bottom one-third of the culture tubes were illuminated. Phototactic cells as well as nonswimming cells accumulated at the bottom of the tube. Approximately 10% of the medium near the top of each tube was enriched for motile cells that could not perform phototaxis and was transferred to new medium. After at least four rounds of enrichment, cells were plated for single colonies, the colonies were transferred to liquid medium, and the phototactic phenotypes were examined. 122 independent phototactic mutant strains were identified from the UV irradiation mutagenesis (Lamb, M., S. Dutcher, and C. Dieckmann, unpublished results).

In the second scheme, an arginine auxotrophic strain, *arg*7-8, was transformed with the pARG7.8 plasmid (Debuchy et al., 1989), which contains the gene for argininosuccinate lyase and confers prototrophy to transformed strains. In *Chlamydomonas*, most transformation events occur by nonhomologous integration into the nuclear genome (Tam and Lefebvre, 1993). 353 transformant strains were selected for arginine prototrophy (Dutcher, S.K., and E. Trabuco, manuscript in preparation), and these strains were screened using the phototaxis assay described above. Four transformed strains that could not perform phototaxis were identified. One of the transformed strains (AT1-116, later designated *pf*9-3) was mapped to the *PF*9/*IDA*1 locus and was given to Dr. M. Porter (University of Minnesota, Minneapolis) for further study.

Phenotypic Analyses

All phenotypic observations were performed on logarithmically growing cells. Eyespot morphology was determined by fixing cells in 2% glutaraldehyde and viewing the cells on an Axiophot microscope (Carl Zeiss, Inc., Thornwood, NY) with a Plan-neofluar ×40 objective. Photoshock behavior was assayed by examining the recorded images of dark-adapted cells that were given a flash of bright light (Hegemann and Bruck, 1989). The cell images were recorded using a high resolution video camera (model NC70; Dage-MTI, Michigan City, IN) and a video cassette recorder (model HR-J62OU; JVC, Elmwood Park, NJ). The images were then viewed on a Trinitron video monitor (model PVM-1353MD; Sony, Park Ridge, NJ). After exposure to the flash of light, the cells stopped forward movement and swam backwards for ~0.5 s. The cells then moved forward again at full velocity. The average swimming velocity of the mutant strains was determined by manually examining the recorded images of swimming cells.

Qualitative motility assessments were performed on a Zeiss microscope using a neofluar ×40 objective. The major feature of the swimming phenotypes assessed was the degree of jerkiness in the movement of individual cells. Different strains had one of three phenotypes based on the degree of jerkiness of the cell body. Wild-type cells had a slightly jerky phenotype where individual cell bodies moved backwards a small degree while the cells were traveling forwards. A very jerky phenotype corre-

sponded to strains where the forward travel of the cell body was interspersed with large backwards movements. Strains that have defects in the outer dynein arms have very jerky cell body movements, which are likely a result of the increased wavelength of the recovery stroke in the beat cycle (Brokaw and Kamiya, 1987). A smooth (or no jerkiness) phenotype was assigned to strains where the cell body moved forward steadily with very little or no discernible backwards movements. Strains that have defects in the inner dynein arm region characteristically had very smooth cell body movements, which are likely to be a result of the reduction of sliding velocities in the forward and recovery strokes (Brokaw and Kamiya, 1987). The motility phenotypes of the following strains were examined and compared to the phototactic mutant strains: *oda*1–*oda*11 (Kamiya, 1988; Sakakibara et al., 1991), *ida*1–*ida*4 (Kamiya et al., 1991), *bop*2, *lis*1, and *lis*2 (Dutcher et al., 1988), *mbo*1–*mbo*3, *pf*1, *pf*2, *pf*3, *pf*9, *pf*10, *pf*12, *pf*14, *pf*17, *pf*18, *pf*25, and *spf*1(previously termed sup_{pf}1) (Harris, 1989). Many of these strains were provided by Dr. Elizabeth Harris of the *Chlamydomonas* Genetics Center (Duke University, Durham, NC).

Cross-sectional electron micrographs of fixed axonemes were prepared as described previously (Porter et al., 1992).

Genetic Analyses

The genetic techniques used for determining the segregation of markers and for mapping the phototactic mutant strains were as described in Harris (1989). Dominance and complementation analyses of the UV irradiation–generated strains were performed using complementing alleles at the *ARG*7 locus and selecting prototrophic diploid strains (Harris, 1989). Dominance and complementation analyses of the DNA insertion–generated strains were performed in diploid strains constructed using the closely linked *ac*17-1 and *nit*2-1 markers in repulsion. Diploid strains were selected on medium that contained no acetate and 2 mM potassium nitrite as the only nitrogen source (Fernández et al., 1989) At least twelve independent diploid strains were examined for each dominance and complementation test. The *pf*18 strain was used as the mating-type partner for the dikaryon analysis as described in Ehler et al. (1995).

Molecular Analyses

The isolation of *Chlamydomonas* genomic DNA and Southern blot hybridization conditions were as described in Johnson and Dutcher (1991). Genomic DNA from the transformant strains were cut with PvuII, SacI, and SalI (Boehringer Mannheim Biochemicals, Indianapolis, IN). A DNA probe for the vector sequences of the pARG7.8 plasmid was made by cutting the 3270-bp restriction fragment of an EcoRI SalI double digest of pARG7.8 from a 0.8% agarose gel. The gel slice was centrifuged at 2,800 *g* for 10 min through a homemade glass wool spin column to remove the DNA fragment from the agarose (Heery et al., 1990). ^{32}P-radiolabeled probes were generated using the RPN1600Z Multiprime DNA Labelling System (Amersham Corp., Arlington Heights, IL). Since the enzymes used to cut the genomic DNA cut pARG7.8 outside the probe sequence, each band seen by Southern analysis corresponded to a fragment of DNA that included genomic DNA and integrated plasmid DNA at the site of pARG7.8 insertion.

Dynein Extraction and Fractionation

Demembranated flagellar axonemes were obtained from large-scale (20–40-liter) cultures of vegetative cells as described previously (Gardner et al., 1994). The axonemes were extracted in 0.6 M NaCl, 0.1 mM ATP, and 10 μM taxol for 15 min on ice and centrifuged at 40,000 *g* for 30 min. The dynein-containing supernatant was collected, and the axonemes were resuspended, extracted, and centrifuged a second time. Both supernatants were pooled and diluted in 9 vol of low salt chromatography buffer (Gardner et al., 1994). The ATPase activity of dynein pool, whole axoneme, and extracted axoneme fractions was determined as described in Gardner et al. (1994). 75–95% of ATPase activity was removed from axonemes after extraction (data not shown). The fractionation of dynein extracts was performed as described by Goodenough et al. (1987) with modifications by Kagami and Kamiya (1992) and Gardner et al. (1994). To confirm the identity of the dynein species, UV irradiation–induced vanadate cleavage was performed on the dynein fractions (Kagami and Kamiya, 1992). Cleavage fragments identical to those described by Kagami and Kamiya (1992) were observed (data not shown). HPLC peaks are designated in capital letters, and dynein complexes are designated in lowercase italic letters (Gardner et al., 1994). Given the biochemical complexity of the inner dynein arms, we opted to use the nomenclature of Kamiya (1995).

Electrophoresis

One-dimensional resolution of the dynein heavy chains and intermediate chains of >120 kD was performed using 3–5% acrylamide gels with a 3–8 M urea gradient (Kamiya et al., 1991). Intermediate chains <120 kD and light chains were resolved on 4–11% acrylamide gels with a 3–9% sucrose gradient. Two-dimensional electrophoresis was performed as described previously (Piperno et al., 1981) with the following modifications. Pharmalytes (Pharmacia Fine Chemicals, Piscataway, NJ) were used in a ratio of 4:6:7 for pH 3–10/pH 6.5–9/pH 4–6.5, respectively. The first-dimension gels were run for 16 h at 1.2 mA constant current. The second-dimension gels contained 5–11% acrylamide and 3–9% sucrose gradients. All gels were silver stained using the method of Blum et al. (1987) with two modifications. First, all gels that contained urea were fixed for several hours, washed once for 60 min in distilled water, and returned to the fixer solution to reduce background staining. Second, the development of all gels was stopped by repeated washes in distilled water. All gels were photographed using a Tiffen 8 YELLOW 2 filter (Tiffen Optical Co., Roslyn Heights, NY).

Phosphatase Treatment

Calf intestinal phosphatase (CIP; Boehringer Mannheim Biochemicals) was used in the provided reaction buffer. Calcineurin (Sigma Chemical Co.) was resuspended into 20 mM Hepes, pH 7.4, 100 mM NaCl, 5 mM $MgSO_4$, and 0.33 mg/ml BSA. Calcineurin was used in 1 mM $CaCl_2$, 1 mM $MnCl_2$, and 5 U of calmodulin (Sigma Chemical Co.) per U of calcineurin. All phosphatase reactions were incubated at 30°C for 60 min.

Sliding Disintegration Assay

Axonemes were collected as described previously (Howard et al., 1994) except that the pH shock method was used to deflagellate the cell bodies (Witman et al., 1972). All axonemes were diluted to 0.85 mg/ml in buffer B (10 mM Hepes, 5 mM $MgSO_4$, 1 mM DTT, 1 mM EGTA, 50 mM potassium-acetate, and 0.5% polyethylene glycol) that contained 0.1 mM PMSF and 0.6 TIU Aprotonin. In the kinase inhibitor experiment, axonemes were treated with 30 μM *N*-(2-guanidinoethyl)-5-isoquinolinesulfonamide hydrochloride (HA-1004; ICN Biochemicals Inc., Irvine, CA) for 15 min on ice. The axonemes were brought to 0.1 mM ATP at room temperature (21–22°C) for 10 min. In all experiments, axonemes were placed into a perfusion chamber and washed with 5 vol of room temperature buffer B that contained 0.1 mM ATP to remove axonemes that did not stick to the glass slide. Sliding disintegration occurred after the chamber was perfused with room temperature buffer B that contained 0.1 mM ATP and 5 μg/ml nagarse (type XXVII protease; Sigma Chemical Co.). The images of disintegrating axonemes were recorded on a video cassette recorder as described above. Frame by frame measurements were made to determine the sliding velocities of the microtubule doublets. Statistical comparisons of mean sliding velocities were performed using an unpaired two-tailed *t* test. *P* values of <0.05 were considered statistically significant.

For several of the strains examined, the percentage of axonemes that disintegrated using 1.0 mM ATP and 2 μg/ml nagarse as described by Howard et al. (1994) was too low to obtain useful measurements. Kurimoto and Kamiya (1991) had noticed that the frequency of disintegration events was decreased in the double mutant *ida*2 *ida*4 at higher ATP concentrations. Therefore, we varied the ATP and nagarse concentrations to find conditions under which a higher percentage of axonemes disintegrated. At 0.1 mM ATP and 5 μg/ml nagarse, we found that ~80% of wild-type axonemes routinely disintegrated, and that there was no significant difference between the sliding velocities of wild-type axonemes at the two conditions ($P = 0.29$). The percentage of axonemes that could slide was determined by counting all sliding events from multiple fields of axonemes (n = 151–230 axonemes). Although our mean sliding velocities for wild-type axonemes were slower than those reported by Howard et al. (1994), the velocities were reproducible in all experiments.

Results

Isolation of Mutant Strains Unable to Perform Phototaxis

Mutant strains that could not perform phototaxis were generated either by UV irradiation or by a DNA insertional mutagenesis procedure (Tam and Lefebvre, 1993).

A microscopic analysis of the 125 phototactic mutant strains showed that 47 of these strains had motility phenotypes when compared with the wild-type strain. The presence of this relatively high percentage of motility phenotypes among the phototactic mutant strains suggested that particular parts of the motility machinery of the flagella were required for phototactic behavior. Since we were ultimately interested in studying dynein regulation, we chose mutant strains that exhibited motility phenotypes for further analysis. Eight phototactic mutant strains were characterized further; these included five ultraviolet irradiation–generated strains and three DNA insertion–generated strains.

Phenotypic Analyses of the Phototactic Mutant Strains

The eyespot morphology and photoshock behavior of the mutant strains were examined to determine if defects existed in the initial steps of the phototaxis signal transduction pathway. All eight mutant strains had a single eyespot that was positioned in the correct location, ~45° from the plane of the flagella and just below the equator of the cell. In a photoshock assay, wild-type cells that are dark adapted will transiently swim backwards when illuminated with a bright light source (Hegemann and Bruck, 1989). Cells from the eight mutant strains transiently swam backwards under the same assay conditions, which indicated that the cells could perceive light and could transmit signals from the eyespot to the flagella (Table I). Independently, Pazour et al. (1995) showed that mutant strains that exhibit abnormal eyespot or photoshock phenotypes have defects in the initial phototactic signaling pathway. Therefore, we concluded that the initial, preflagella steps of the phototaxis signal transduction pathway were unlikely to be affected in these eight mutant strains.

The motility phenotypes of the mutant strains were analyzed in two assays (Table I). In the first assay, the average swimming velocities of the mutant strains were determined. The average swimming velocities of the phototactic mutant strains ranged from about one-half to one-third the velocity of the wild-type strain. The second assay was a qualitative assessment of the overall swimming patterns of the mutant cells compared with the motility phenotypes of wild-type and other mutant strains. The cell bodies of isolates 7-1 and 13-5 exhibited a slightly jerky phenotype (see Materials and Methods). This phenotype was similar to the swimming pattern of wild-type strains and was clearly different from the swimming pattern of *oda*$^-$ cells. The overall motility phenotypes exhibited by 7-1 and 13-5 cells (slow swimming velocities and slightly jerky cell body movement patterns) were not seen in any of the other mutant strains examined (data not shown), and therefore were novel. The remaining phototactic mutant strains had smooth cell movement patterns. The overall motility phenotypes resembled previously characterized inner dynein arm region mutant strains.

Table I. Phenotypic Analyses of Phototactic Mutant Strains

Isolation name	Phototaxix phenotype*	Eyespot morphology	Photoshock response	Swimming velocity‡	Motility phenotype§
wild-type	+	+	+	152.1 ± 24.8	slightly jerky
7-1	−	+	+	49.6 ± 13.1	slightly jerky
13-5	−	+	+	63.4 ± 13.0	slightly jerky
AT1-2	−	+	+	61.5 ± 8.4	smooth
AT1-25	−	+	+	73.5 ± 11.6	smooth
AT2-121	−	+	+	80.6 ± 13.7	smooth
8-10	−	+	+	77.1 ± 12.8	smooth
8-14	−	+	+	73.9 ±12.9	smooth
14-9	−	+	+	73.8 ± 10.4	smooth

*Strains that could perform phototaxis (+) were typically concentrated six- to eightfold in the lighted portion of the assay tube compared with the darkened portion. Strains unable to perform phototaxis (−) were found equally dispersed in the lighted and darkened portions of the tube.
‡μm/s ± SD, n = 40–81 cells.
§Qualitative motility assessment as described in Materials and Methods.

Genetic Analyses of the Phototactic Mutant Strains

Genetic analyses were performed on the mutant strains (Table II). The phototactic and motility phenotypes always cosegregated and showed $2^+ : 2^-$ segregation in meiotic progeny. Arginine prototrophy cosegregated with the phototactic and motility phenotypes in the three DNA insertion–generated strains. AT2-121 and AT1-25 isolates contained a single copy of the inserted DNA, while the AT1-2 isolate contained two copies of the inserted DNA (Fig. 1). The inserted DNA segregated with the phototactic, motility, and arginine prototrophy phenotypes in 18 random spores from each of the DNA insertion–generated strains (data not shown). The dominance of the mutations was tested both in stable diploid strains and in temporary dikaryon strains, which briefly share cytoplasm before the fusion of the nuclei from the parental cells of opposite mating–types. The dikaryon strain analyses were performed to determine if the wild-type gene products were present in gametic cells. All eight mutations were recessive in both diploid and dikaryon strains, which indicated that the wild-type alleles were dominant and that the wild-type gene products were present in gametic cells of the mating-type partner. The 8-10 mutation failed to recombine with the 8-14 (55 tetrads) or 14-9 (25 tetrads) mutations. Diploid strains that contained heterozygous combinations of these three mutations were all unable to perform phototaxis (data not shown). Therefore, the 8-10, 8-14, and 14-9 mutations were allelic.

The phototactic mutant strains were mapped to determine if any mutations were allelic with other previously

Table II. Genetic Analyses of Phototactic Mutant Strains

Isolation name	Allele designation	Ptx$^-$/Mot$^-$ segregation*	Ptx$^-$/Arg$^+$ segregation‡	Map position
7-1	*mia*1-1	136	−	L.G. II (24:0:0 to *act*1)
13-5	*mia*2-1	119	−	L.G. XVIII (31:0:6 to *spr*1)
AT1-2	*pf*9-4	56	21	L.G. XII/XIII (32:0:0 to *pf*9)
AT1-25	*ptm*1-1	70	29	L.G. II (73:0:8 to *fsr*1)
AT2-121	*ptm*2-1	52	21	Unknown§
8-10	*ptm*3-1	102	−	L.G. XVIII (61:2:14 to *spr*1)
8-14	*ptm*3-2	43	−	L.G. XVIII‖
14-9	*ptm*3-3	25	−	L.G. XVIII‖

*Number of tetrads in the phototaxis (Ptx$^-$) and motility (Mot$^-$) phenotypes segregated together and as 2^+:2^-.
‡Number of tetrads in which the phototaxis (Ptx$^-$) and arginine prototrophy (Arg$^+$) phenotypes segregated together and as 2^+:2^-.
§This mutation did not show linkage to other genetic markers, but was centromere linked based on mapping to *ac*17 (8:7:0) and *pyr*1 (10:5:0).
‖These mutations were not directly mapped because complementation and recombination analyses described in the text showed that they were allelic with the *ptm*3-1 mutation.

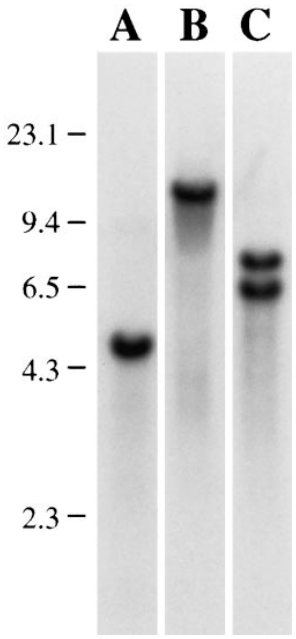

Figure 1. Scanned image of a genomic Southern blot that contains DNA from three mutant strains. The blot was probed with a radiolabeled pARG7.8 vector fragment. SalI restriction endonuclease–digested AT2-121 (*A*) and AT1-25 (*B*) genomes contained a single insertion, whereas the AT1-2 (*C*) genome contained two insertions. (*Left*) Positions of size standards in kb.

characterized mutations. The AT1-2 mutation was tightly linked to the *PF*9/*IDA*1 and *IDA*4 loci on the left arm of linkage group XII/XIII (Dutcher et al., 1991; Porter et al., 1992). Complementation analyses were performed between AT1-2 and the *pf*9-2 or *ida*4-1 alleles. The AT1-2 mutation failed to complement the *pf*9-2 allele, but complemented the *ida*4-1 allele. Therefore, AT1-2 was a new allele at the *PF*9/*IDA*1 locus and was designated *pf*9-4. The map positions of the other phototactic mutations were not near known motility loci, and therefore did not appear to be allelic with other previously mapped mutations. The phototactic mutant strains were all given locus designations (Table II). Based on phenotypes described below, the 7-1 and 13-5 isolates were named *mia*1-1 and *mia*2-1, respectively, for *m*odifiers of *i*nner *a*rms. The remaining isolates were named *ptm*1–*ptm*3 for *p*hototaxis and *m*otility.

Previous work showed that the phenotypic analysis of double mutant strains can help determine relationships between affected structures or functions in mutant strains. Many double mutant strains containing defects in separate dynein classes or other axonemal structures have synthetic or additive phenotypes compared with those of either parental mutant strain (Piperno et al., 1990; Kamiya et al., 1991; Porter et al., 1992; King et al., 1994). Double mutant strains in which each mutation affects the same structure or function usually show a phenotype that is indistinguishable from that of one or both of the parental strains (Kamiya, 1988; Kamiya et al., 1991). *oda*2-1 mutant axonemes have no outer dynein arms (Kamiya, 1988); the cell bodies show a very jerky movement phenotype but are able to perform phototaxis. Three of the eight mutant strains, *mia*1-1, *mia*2-1, and *pf*9-4, had synthetic phenotypes in combination with *oda*2-1. *mia*1-1 *oda*2-1 and *mia*2-1 *oda*2-1 strains had short paralyzed flagella, whereas the *pf*9-4 *oda*2-1 strain was primarily aflagellate with rare flagella that were short and paralyzed (Table III). The other five *ptm*$^-$ strains showed additive phenotypes in combination with the *oda*2-1 mutation. The double mutant cells swam with the characteristic Oda$^-$ motility phenotype but were unable to perform phototaxis.

Since the double mutant strains that contained the *mia*1-1, *mia*2-1, or *pf*9-4 mutations exhibited synthetic phenotypes, double mutant strains were constructed between these three strains and other strains missing various dynein arm region components to ask if other synthetic interactions existed. The *pf*9-4 allele behaved identically to the *pf*9-2 allele when crossed to other inner arm region mutant strains (Porter et al., 1992). In combination with non-*f* inner dynein arm mutant strains, *pf*9-4 had additive or synthetic motility phenotypes that ranged from a slower swimming velocity to the presence of short paralyzed flagella. Double mutant strains of *pf*9-4 in combination with *ida*2-1 or *ida*3-1 were indistinguishable from the parental strains. Double mutant strains between the *mia*1-1 or *mia*2-1 mutations and the *ida*4-1, *pf*2-1, *pf*3-1, or *bop*2-1 mutations exhibited additive or synthetic motility phenotypes that ranged from slower swimming to the assembly of paralyzed flagella (Table III). Double mutant strains between the *mia*1-1 or *mia*2-1 mutations and the *f* inner arm mutant strains (*pf*9-2, *ida*2-1, or *ida*3-1) had the same motility phenotype as the *f* inner arm mutant strain; the characteristic slightly jerky motility phenotypes of the *mia*1-1 or *mia*2-1 mutant strains were not observed. Therefore, the *pf*9-4 mutation was likely to affect the *f* inner dy-

Table III. Genetic Interactions between Dynein Arm Mutations and the mia1-1, mia2-1, and pf9-4 Mutations

Strain*	Motility	Double mutant motility phenotype with		
		mia1-1	*mia2-1*	*pf9-4*
*oda*2-1	slow, very jerky	short, paralyzed	short, paralyzed	rare, short, paralyzed
*ida*4-1	slow, smooth	paralyzed	paralyzed	ND
*pf*2-1	slow, smooth	paralyzed	paralyzed	short, paralyzed
*pf*3-1	slow, smooth	paralyzed	paralyzed	short, paralyzed
*bop*2-1	slow, smooth	very slow	very slow	very slow
*pf*9-2	slow, smooth	slow, smooth	slow, smooth	ND
*ida*2-1	slow, smooth	slow, smooth	slow, smooth	slow, smooth
*ida*3-1	slow, smooth	slow, smooth	slow, smooth	slow, smooth

*The *oda*2-1 strain is missing the outer dynein arms (Kamiya, 1988); the *ida*4-1 strain is missing *a*, *c*, and *d* inner dynein arms (Kagami and Kamiya, 1992); the *pf*2-1 strain is missing components of the drc and has reduced amounts of *b* and *e* inner dynein arms (Huang et al., 1982*a*; Gardner et al., 1994); the *pf*3-1 strain is missing components of the drc and *e* inner dynein arms (Huang et al., 1982*a*; Gardner et al., 1994); the *bop*2-1 strain is missing radially asymmetric inner dynein arm structures (King et al., 1994); and the *pf*9-2, *ida*2-1, and *ida*3-1 strains are missing the *f* inner dynein arms (Kagami and Kamiya, 1992; Porter et al., 1992).
ND, not determined because of the absence of recombinants.

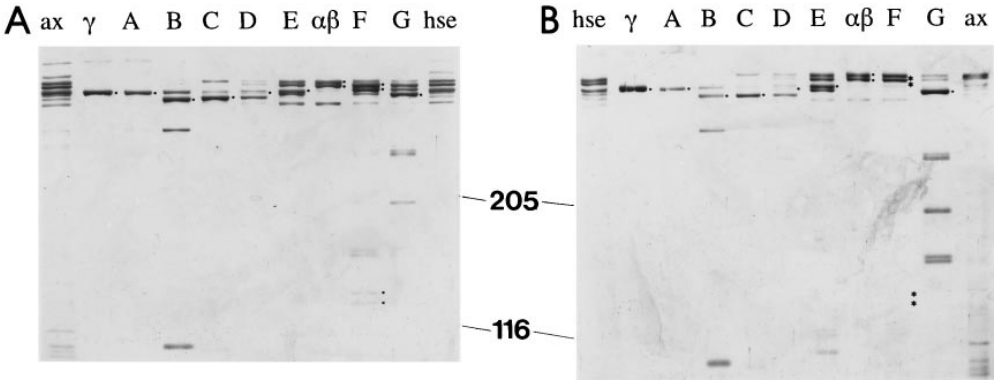

Figure 2. Silver-stained SDS-PAGE gels of the HPLC-fractionated dynein heavy and intermediate chains from wild-type (*A*) and *pf*9-4 (*B*) axonemes. The HPLC fractions are labeled for each lane. *hse*, high salt extract; *ax*, whole axonemes. Several dynein peaks contained polypeptides from neighboring dynein peaks. The polypeptides that were part of the particular complex separated in each peak are labeled with a dot on the right of the band. The F fraction of *pf*9-4 dynein extracts was missing two heavy and three intermediate *f* dynein polypeptides; the expected positions of these bands are shown by asterisks. This gel did not resolve the 110-kD *f* intermediate chain, but it was missing in other gels (data not shown). The positions of 205- and 116-kD standards are indicated.

nein arms, and the *mia*1-1 and *mia*2-1 motility phenotypes appeared to require the presence of the *f* dynein complex.

Dynein Composition of the Phototactic Mutant Strains

To determine if the axonemal dynein composition was altered in the mutant strains, dynein extracts from mutant axonemes were fractionated by ion-exchange HPLC over a Mono-Q column. The polypeptides of the fractions were then separated by SDS-PAGE. The dynein fractions were distinguished based on the identity of the dynein heavy chains present. In wild-type dynein extracts, the eight inner arm dynein heavy chains were separated into seven distinct inner arm complexes named *a–g* (Fig. 2; Kagami and Kamiya, 1992). The outer arm dynein was separated into two fractions: one that contained the γ dynein heavy chain, and one that contained the α and β heavy chains (Fig. 2; Gardner et al., 1994).

None of the five *ptm*$^-$ strains had detectable defects in dynein composition by this assay and were not analyzed further. The three other mutant strains, *pf*9-4, *mia*1-1, and *mia*2-1, had defects in the *f* inner arm dynein complex. *pf*9-4 axonemes were missing the entire *f* inner arm dynein complex (Fig. 2). The two dynein heavy chains and the three intermediate chains of 140, 138, and 110 kD were totally absent. The other polypeptides in the F fraction were not components of the *f* dynein complex and are from the shoulders of the αβ and G fractions. This *pf*9-4 dynein phenotype was identical to the previously reported phenotypes of other *pf*9/*ida*1 alleles (Kagami and Kamiya, 1992; Porter et al., 1992).

*mia*1-1 and *mia*2-1 fractionated dynein extracts showed a change in the electrophoretic mobility of intermediate weight polypeptides of the *f* dynein complex as compared with wild-type *f* dynein (Fig. 3). In *f* dynein extracted from wild-type axonemes, the 138- and 140-kD intermediate chains were prominent, and a slight smear was seen extending upward from the 138-kD polypeptide. In *f* dynein extracted from *mia*1-1 axonemes, a new polypeptide species was observed that migrated between the 138- and 140-kD intermediate chains, and the smear extending up from the 138-kD polypeptide showed increased intensity. In *mia*2-1 *f* dynein extracts, the amount of the 138-kD intermediate chain was greatly reduced: a new, slower migrating polypeptide was observed. Increased smearing was also observed. The 140- and 110-kD intermediate chains and the two heavy chains of the *f* inner arm complex were not affected by the *mia*1-1 or *mia*2-1 mutations (data not shown). These polypeptide phenotypes were reproduced in multiple preparations of *mia*1-1 and *mia*2-1 axonemes from at least three independent meiotic segregants. Therefore, both *mia*1-1 and *mia*2-1 axonemes contained alterations in an intermediate chain of the *f* inner dynein arm complex.

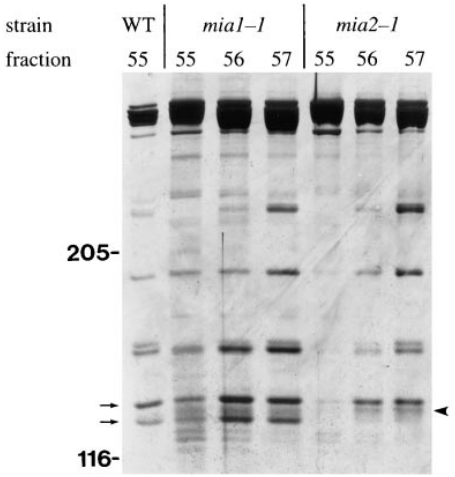

Figure 3. Silver-stained gel showing HPLC fractionated polypeptides from wild-type, *mia*1-1, and *mia*2-1 dynein extracts. One fraction of wild-type and three consecutive fractions of *mia*1-1 and *mia*2-1 extracts are shown. Polypeptides of the αβ outer arm and *g* inner arm dyneins cofractionated to some extent with *f* dynein (Fig. 2; Kagami and Kamiya, 1992; Gardner et al., 1994). The wild-type fraction was underloaded compared with the other fractions. When wild-type fractions were overloaded, no additional bands were observed as in *mia*$^-$ fractions. (*Arrows*, *left*) Positions of the 140-kD and 138-kD intermediate chains of the wild-type *f* dynein complex. (*Arrowhead*, *right*) Position(s) of the new polypeptide species seen in *mia*1-1 and *mia*2-1 dynein extracts. The positions of 205- and 116-kD standards are indicated.

Since the three strains with phototaxis defects all had defects in the *f* inner dynein arm complex, we assayed phototactic behavior for three mutant alleles at the *PF*9/*IDA*1 locus and one mutant allele at the *IDA*2 and *IDA*3 loci, which all result in the complete loss of the *f* inner dynein arm complex (Kamiya et al., 1991; Porter et al., 1992). The Ida^- motility phenotype cosegregated with the Ptx^- phenotype in meiotic crosses of the three loci in 97, 40, and 41 tetrads, respectively. The loss of phototactic ability was not simply a result of having a motility phenotype. Mutant strains that have defects in the outer dynein arms (*oda*1–*oda*10), dynein regulatory complex (drc) (*pf*2 and *pf*3), or non-*f* inner dynein arm complexes (*ida*4, *pf*3, *bop*2) were able to perform phototaxis even though the strains had swimming phenotypes comparable to those of *f* inner dynein arm mutant strains (data not shown). These results suggested that the *f* inner dynein arm complex was required directly or indirectly for correct phototactic behavior.

Altered Phosphorylation of the 138-kD Polypeptide in mia1-1 and mia2-1 Axonemes

*mia*1-1 and *mia*2-1 *f* inner dynein arm fractions were analyzed further to determine the nature of the biochemical defect. Previous results had shown that the 138-kD polypeptide is the only phosphoprotein in the *f* inner dynein arm complex (Piperno and Luck, 1981; Habermacher and Sale, 1996). Therefore, we reasoned that the new polypeptides present in *mia*1-1 and *mia*2-1 dynein extracts could be phosphorylation modifications of the 138-kD polypeptide. To test this hypothesis, *f* inner dynein arm complexes from the wild-type, *mia*1-1, and *mia*2-1 strains were treated with CIP. The faint smear of slower migrating polypeptides observed in untreated wild-type preparations disappeared, and the 138-kD band appeared more intense after CIP treatment (Fig. 4 *A*). When *mia*1-1 and *mia*2-1 *f* inner dynein arm complexes were treated with CIP, the extra polypeptide(s) and the increased smears disappeared and the 138-kD polypeptide band was more prominent. These polypeptide mobility shifts did not occur in the presence of vanadate ions, which are a potent inhibitor of phosphatases (Gordon, 1991). After addition of CIP, the electrophoretic mobilities of the *f* dynein intermediate polypeptides from *mia*1-1 and *mia*2-1 dynein preparations were comparable to the mobility of the wild-type *f* dynein intermediate polypeptides. These results suggested that the intermediate chain mobility phenotypes observed in mia^- *f* dynein extracts resulted from altered phosphorylation of the 138-kD polypeptide, and that the 138-kD polypeptide phosphorylation state was altered to a greater degree in *mia*2-1 dynein extracts than in *mia*1-1 dynein extracts.

Calcineurin, which is a Ca^{++}- and calmodulin-depen-

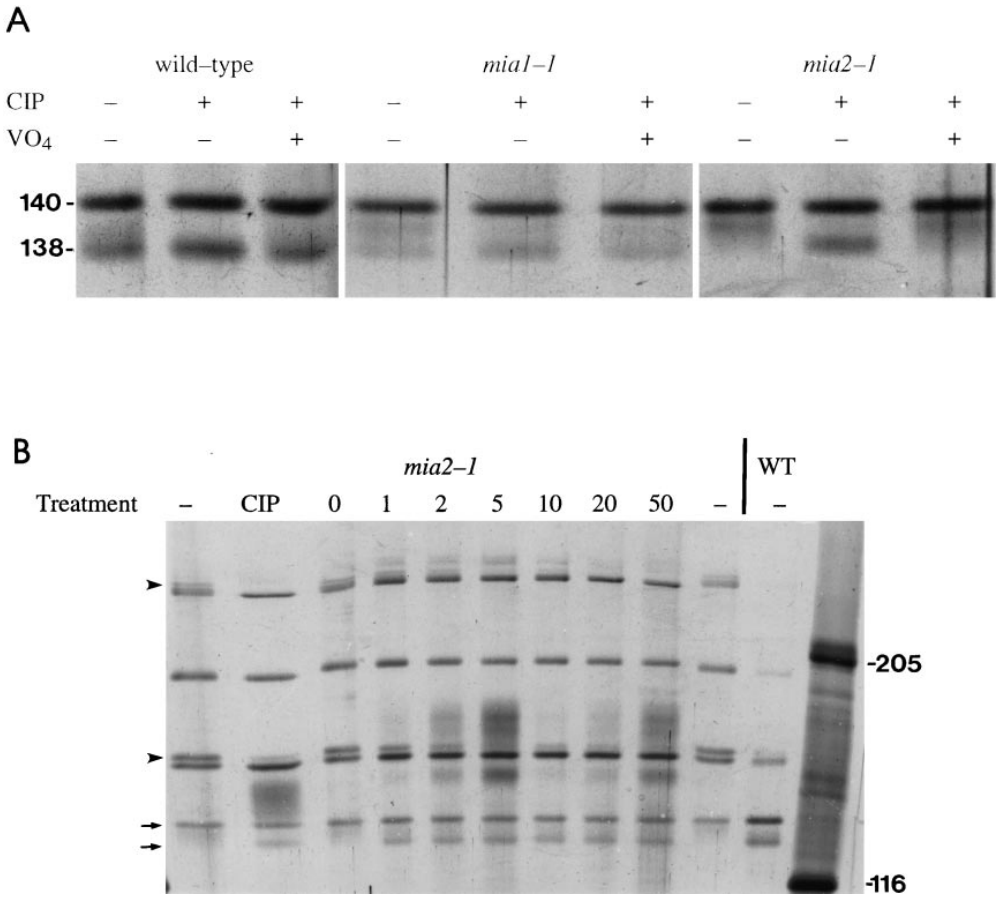

Figure 4. Phosphatase treatment alters the electrophoretic mobility of *f* dynein polypeptides. (*A*) Silver-stained gels of the *f* dynein polypeptides from wild-type, *mia*1-1, and *mia*2-1 dynein extracts after treatment with CIP. Only the region of the gel that contained the *f* dynein 140- and 138-kD intermediate polypeptides is shown. The wild-type lanes were overloaded to show the faint smear of polypeptides that extended upward from the 138-kD polypeptide. Positions of the 140- and 138-kD polypeptides (*left*). The presence (+) or absence (−) of phosphatase (*CIP*) and 5 μM sodium orthovanadate (VO_4) is indicated. (*B*) Silver-stained gel showing the electrophoretic mobility of F fraction polypeptides. The dynein heavy chains are not shown. The far right lane contains 205- and 116-kD standards. The next to last lane on the right contains wild-type F fraction polypeptides. The remaining lanes contain equal amounts of *mia*2-1 F fraction polypeptides. Phosphatase addition is indicated above each lane; −, no treatment; *CIP*, calf intestinal phosphatase treatment; calcineurin treatment, numbers correspond to units of calcineurin added. (*Arrows*) Positions of the 140- and 138-kD polypeptides. The migration of two additional non-*f* dynein polypeptides was affected by calcineurin treatment; these bands are indicated by arrowheads.

dent type 2B protein phosphatase, is present in spermatazoa flagella from a variety of species and has been found in *Chlamydomonas* flagella (Tash, 1989). The F fractions from a *mia*2-1 dynein extract were incubated with calcineurin. The severe *mia*2-1 138-kD intermediate chain phenotype was rescued in the presence of exogenous calcineurin as it was in the presence of CIP (Fig. 4). Interestingly, the 138-kD intermediate chain appeared to be a better substrate for calcineurin relative to the other non-*f* dynein polypeptides present in the HPLC fraction. The full effect of calcineurin dephosphorylation on the mobility of the 138-kD intermediate chain was observed at the lowest concentration of calcineurin, whereas much higher concentrations of calcineurin were needed to affect the mobility of other non-*f* dynein polypeptides present (Fig. 4 *B*). On the other hand, CIP addition shifted the mobilities of several non-*f* dynein fraction polypeptides at a low concentration (Fig. 4, lane *2*). Since calcineurin is known to have very narrow substrate specificity (Cohen, 1982), these results suggest that calcineurin could be the endogenous phosphatase that dephosphorylates the 138-kD intermediate chain.

mia1-1 and mia2-1 Axonemes Have Additional Polypeptide Defects

Previous results have suggested that defects in the radial spokes and central pair microtubules may lead to increased phosphorylation of an inner arm component (Howard et al., 1994; Habermacher and Sale, 1996). We used two-dimensional gel analysis to ask if the radial spokes or central pair microtubules were affected in the *mia*$^-$ strains. None of the known radial spoke or central pair polypeptides were visibly affected. *mia*1-1 and *mia*2-1 axonemes were also examined by standard EM techniques. All *mia*1-1 and *mia*2-1 axonemal structures appeared normal (data not shown).

Although *mia*1-1 and *mia*2-1 axonemes did not have detectable defects in the radial spokes or central pair microtubules, the two-dimensional gel analysis identified other axonemal polypeptide assembly defects. *mia*1-1 axonemes lacked a 74-kD polypeptide (Fig. 5). In both *mia*1-1 and *mia*2-1 axonemes, a polypeptide of ~34 kD was reduced or absent (Fig. 6). The 74- and 34-kD polypeptides are present in axonemes lacking the central pair microtubules (Adams et al., 1981; Dutcher et al., 1984), radial spokes (Piperno et al., 1977, 1981), dynein arms (Huang et al., 1979; Piperno and Luck, 1981), B-tubule projections (Segal et al., 1984), drc (Huang et al., 1982*a*; Piperno et al., 1992), and in the *ptx*1 strain (Horst and Witman, 1993). The *mia*$^-$ strains are the first to be missing these two polypeptides. In *mia*2-1 axonemes, a 35-kD polypeptide was reduced or missing, and a novel polypeptide, which was not present in wild-type preparations, was observed. Unexpectedly, the 35-kD polypeptide was missing in axonemal preparations from the *pf*9-2 strain (Fig. 6 *B*). The 35-kD polypeptide was not high salt extractable (data not shown), and therefore was not likely to be a component of the extractable *f* inner dynein arm. Flagellar preparations, which were comprised of axonemal, matrix, and membrane components, were examined. No differences besides the axonemal differences were observed between wild-type and *mia*1-1 or *mia*2-1 preparations (data not shown).

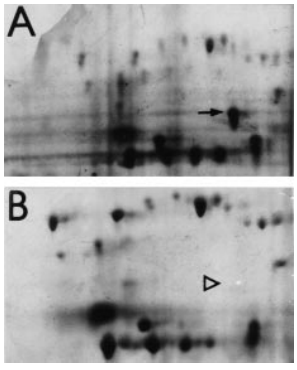

Figure 5. The 74-kD region of silver-stained two-dimensional gels. (*Arrow*) Position of the 74-kD polypeptide in wild-type axonemes (*A*); (*arrowhead*) expected position in *mia*1-1 axonemes (*B*). All two-dimensional gels are shown with acidic pIs to the right. Other polypeptide variability seen in the two-dimensional gels of Figs. 5–7 was not consistent in other gels and in other axonemal preparations.

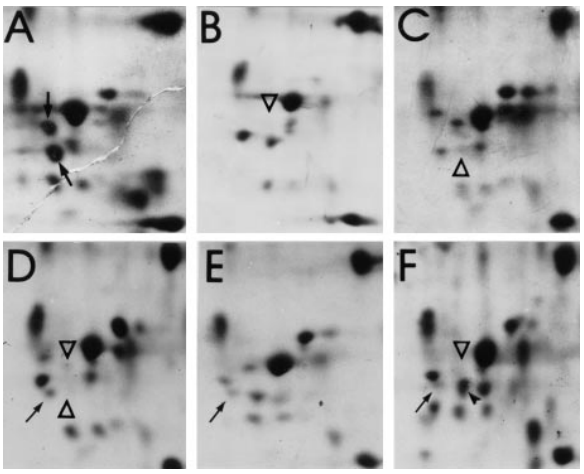

Figure 6. The 35-kD region of silver-stained two-dimensional gels of axonemes from different strains. (*A*) wild-type; (*B*) *pf*9-2; (*C*) *mia*1-1; (*D*) *mia*2-1; (*E*) wild-type and *mia*2-1; (*F*) *mia*2-1R-14. (*A*, *arrows*) Positions of the 35- and 34-kD polypeptides discussed in the text. (*open arrowheads*, *pointing down*) Expected position of the 35-kD polypeptide. (*open arrowheads*, *pointing up*) Expected position of the 34-kD polypeptide. (*D*, *E*, and *F*, *small arrows*) Positions of the novel polypeptide found in *mia*2-1 axonemes. (*F*, *black arrowhead*) Return of the 34-kD polypeptide in *mia*2-1R-14 axonemes.

To further examine the electrophoretic mobility of the novel polypeptide seen in *mia*2-1 axonemes, we loaded equal amounts of wild-type and *mia*2-1 axonemes onto the same gel (Fig. 6 *E*). The 35- and 34-kD polypeptides contributed from wild-type axonemes were present. The novel polypeptide had a more basic pI and a slightly slower migration than the wild-type 34-D polypeptide.

The mobilities of the 138- and 140-kD polypeptides were examined on two-dimensional gels. Goodenough et al. (1987) examined HPLC-fractionated inner dynein arms and were the first to show that both 138- and 140-kD polypeptides were part of an inner dynein arm complex. A faint series of at least six spots that are present in wild-type axonemes was missing in *pf*9-2 axonemes (Fig. 7). These spots correspond to the approximate location of the 138-kD polypeptide shown by Goodenough et al. (1987) and Luck and Piperno (1989). Neither we nor Luck and Piperno were able to identify the 140-kD polypeptide in two-

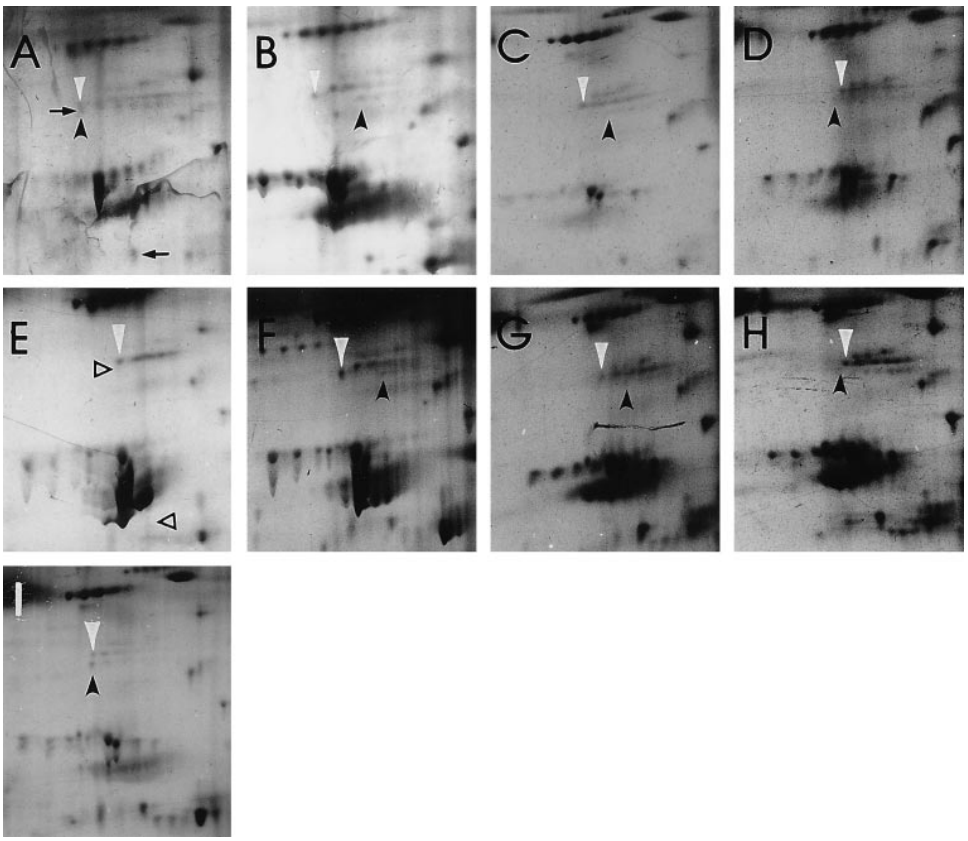

Figure 7. The 138-kD region of silver-stained two-dimensional gels of axonemes from different strains. (*A*) wild-type; (*B*) *mia*1-1; (*C* and *D*) *mia*1-1 *spf*1-1; (*E*) *pf*9-2; (*F*) *mia*2-1; (*G* and *H*) *mia*2-1 *spf*1-1; (*I*) *mia*2-1R-14. The axonemes in *D* and *H* were treated with HA-1004. (*Arrows*) Positions of the 138- and 110-kD *f* polypeptides in wild-type axonemes (*A*). The series of 138-kD polypeptide spots is found just below a more prominent axonemal polypeptide series. (*Filled arrowheads*) Position of the most basic form of the 138-kD polypeptide found in the corresponding axonemes. (*Open arrowheads*) Expected positions of the 138- and 110-kD polypeptides in *pf*9-2 axonemes (*E*).

dimensional gels of axonemal preparations. This polypeptide was located at the pI of tubulin and may be obscured (data not shown; Goodenough et al., 1987). In axonemes from the *mia*$^-$ strains, the 138-kD polypeptide series was shifted to a more acidic pI relative to other axonemal polypeptides. Therefore, the altered phosphorylation phenotypes identified in one-dimensional gels of the *mia*$^-$ strains (Fig. 4) were likely to be a result of increased phosphorylation levels of the 138-kD polypeptide.

Dynein Activity of mia1-1 and mia2-1 Axonemes

We used a modification of the sliding disintegration assay developed by Okagaki and Kamiya (1986), Kurimoto and Kamiya (1991), and Howard et al. (1994) to determine if dynein activity was altered in the *mia*1-1 and *mia*2-1 mutant strains. The sliding velocities of wild-type, *mia*1-1, and *mia*2-1 axonemes were not statistically different from each other in the presence of the outer dynein arms (Table IV). To ask if the sliding disintegration assay could detect axonemal dynein activity differences that were a result of the complete absence of the *f* inner arms, we measured the sliding velocity of *pf*9-2 axonemes. *pf*9-2 axonemes had a sliding velocity that was significantly slower than that of wild-type (P = 8.0 x 10^{-8}), *mia*1-1 ($P = 3.3 \times 10^{-4}$), or *mia*2-1 ($P = 3.3 \times 10^{-5}$) axonemes. Therefore, *mia*1-1 and *mia*2-1 axonemes did not have dynein defects that were comparable to the loss of the entire *f* dynein complex.

We expected that only inner dynein arm activity would be affected in the *mia*$^-$strains and that outer dynein arm activity may have masked slight differences in the activity of the inner dynein arms. Therefore, we examined the axonemal sliding velocities of the *mia*$^-$ mutant strains in the genetic background of mutations that affected outer dynein arms. We used either the *oda*2-1 mutation, which results in the loss of the entire outer dynein arm (Kamiya, 1988), or the *spf*1-1 mutation, which results in the assembly of outer dynein arms with a seven–amino acid deletion in the β heavy chain (Huang et al., 1982*a*; Porter et al., 1994). *oda*2-1 axonemes were full length and had a mean sliding velocity that was significantly slower than that of the wild-type sliding velocity (Table IV). However, *mia*1-1 *oda*2-1 and *mia*2-1 *oda*2-1 axonemes only rarely disintegrated (Table IV), which was likely to be related to the synthetic, short flagellar length phenotype of these strains (Table III). Because so few *mia*$^-$ *oda*2-1 axonemes disintegrated, we were unable to determine mean sliding velocities for these double mutant strains.

Table IV. Microtubule Sliding Velocities from Axonemes of Various Strains

Strain (*n*)	Percentage of axonemes that slide	Mean sliding velocity	Significance*
	%	*μm/s ± SD*	
wild-type (48)	81.0	12.61 ± 2.46	ND
*mial*1-1 (28)	36.2	11.83 ± 2.79	$P = 0.31$
*mial*1-1 (28)	39.1	11.42 ± 3.21	$P = 0.41$
*pf*9-2 (14)	24.5	9.50 ± 1.19	$P = 8 \times 10^{-8}$
*oda*2-1 (15)	11.2	4.29 ± 0.40	$P = 4 \times 10^{-29}$
*mia*1-1 *oda*2-1	< 1	ND	ND
*mia*2-1 *oda*2-1	< 1	ND	ND

*Compared with the distribution of the velocities of wild-type axonemes.

*spf*1-1 single and double mutant strains had full-length flagella, and >20% of the axonemes from these strains disintegrated. *spf*1-1 axonemes had a mean sliding velocity (Fig. 8) that was significantly faster than that of *oda*2-1 axonemes ($P = 7.8 \times 10^{-9}$), but slower than that of wild-type axonemes ($P = 2.5 \times 10^{-25}$). These data suggested that the outer dynein arm activity in *spf*1-1 axonemes was reduced but not absent. *spf*1-1 sliding velocities had previously been reported to be comparable to wild-type values (Porter et al., 1994). *mia*1-1 *spf*1-1 and *mia*2-1 *spf*1-1 sliding velocities were slower than the sliding velocities of *spf*1-1 axonemes, and *mia*2-1 *spf*1-1 sliding velocities were slower than those of *mia*1-1 *spf*1-1 axonemes (Fig. 8). Therefore the *mia*$^-$ mutations caused a reduction in axonemal dynein activity, but this reduction was not as severe as the loss of the entire *f* inner dynein arm complex.

To ask if the reduced dynein activity in the sliding disintegration assay resulted from altered phosphorylation of the 138-kD *f* inner dynein arm polypeptide, kinase inhibitor was added to *spf*1-1, *mia*1-1 *spf*1-1, and *mia*2-1 *spf*1-1 axonemes. The kinase inhibitor HA-1004, which competes with ATP for free cAPK (Hidaka et al., 1984), increases the sliding velocities of various mutant strains in sliding disintegration assays (Howard et al., 1994). The sliding velocity of *spf*1-1 axonemes was not affected by HA-1004 treatment (Fig. 8). The sliding velocity of treated *mia*1-1 *spf*1-1 axonemes increased and was not significantly different than that of treated *spf*1-1 axonemes (Fig. 8). Interestingly, while the sliding velocity of treated *mia*2-1 *spf*1-1 axonemes increased to a level that was not significantly different from that of treated *mia*1-1 *spf*1-1 axonemes, the velocity remained significantly different from that of treated *spf*1-1 axonemes (Fig. 8). We concluded that the addition of kinase inhibitor fully restored activity to *mia*1-1 *spf*1-1 axonemes and partially restored activity to *mia*2-1 *spf*1-1 axonemes.

The phosphorylation states of the 138-kD polypeptide were examined by two-dimensional gel electrophoresis for both control and treated *mia*1-1 *spf*1-1 and *mia*2-1 *spf*1-1 axonemes. In treated axonemes from both strains, the 138-kD polypeptide series was shifted to a more basic pI relative to other axonemal polypeptides (Fig. 7, *D* and *H*). The new mobility of the 138-kD polypeptide series was comparable to the position seen in wild-type axonemes (Fig. 7 *A*). The relative mobilities of other axonemal polypeptides were not shifted after HA-1004 treatment (data not shown). Therefore, HA-1004 treatment resulted in a shift in the mobility of the 138-kD polypeptides toward the wild-type positions, and this shift was concurrent with an increase in inner dynein arm activity.

Coreversion of Phenotypes

To ask if the multiple phenotypes exhibited by the *mia*$^-$ strains were related, we examined revertants of the *mia*$^-$ mutations. A single intragenic revertant (*mia*2-1*R*-14) of the *mia*2-1 mutation was isolated (King, 1996). The *mia*2-1*R*-14 strain was wild type for both the phototaxis and swimming phenotypes. Two-dimensional gel electrophoresis of *mia*2-1*R*-14 axonemes showed that the 34- (Fig. 6 *F*) and 138-kD (Fig. 7 *I*) polypeptide phenotypes also reverted. The novel polypeptide was still present and the 35-kD polypeptide was still reduced in *mia*2-1*R*-14 axonemes (Fig. 6 *F*). Therefore, the loss of the 35 kD and the appearance of the novel polypeptide phenotypes were not sufficient to cause Mia$^-$ phenotypes.

Asymmetric Localization of 138-kD Polypeptide Species

Rüffer and Nultsch (1991) showed that the waveforms of the *cis* and *trans* flagella are altered coordinately to maneuver the cell during phototactic turning. To ask if the 138-kD polypeptide had different levels of phosphorylation in *cis* or *trans* flagella, dynein extracts from *uni*1-1 axonemes were fractionated by HPLC (Fig. 9), and both a new polypeptide band and an increased smear of polypeptides were observed in the 138-kD region. Greater than 99% of the flagella in this preparation of *uni*1-1 axonemes were *trans* relative to the eyespot (data not shown; Huang et al., 1982*b*). This biochemical phenotype was remarkably similar to that seen in *mia*1-1 dynein extracts (Fig. 3). Based on the similarity of the phenotypes of *mia*1-1 and *uni*1-1 *f* dynein complexes, it seems likely that the *f* inner

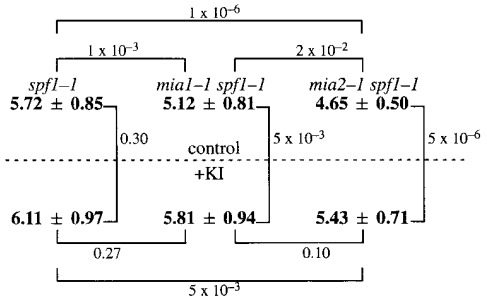

Figure 8. Sliding velocities of axonemes from various strains. The sliding velocities (in μm/s ± SD) of axonemes without (*top values*; labeled *control*) and with HA-1004 (*bottom values*; labeled ±*KI*) treatment are shown in bold type. The value by each bracket is the *P* value of an unpaired two-tailed *t* test between the corresponding sliding velocity distributions. *P* values of <0.05 were considered significant. 27–31 independent events were measured for each condition.

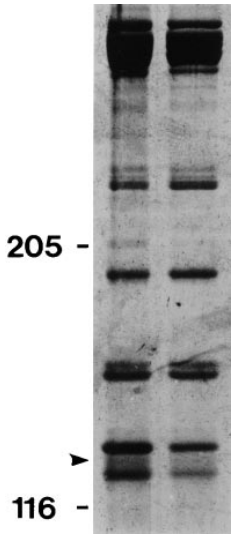

Figure 9. Silver-stained gel showing HPLC-fractionated polypeptides from *uni*1-1 dynein extracts. Two consecutive fractions are shown. (*Arrowhead*) Positions of the new polypeptide species seen in the dynein extract. The 138-kD polypeptide phenotype in *uni*1-1 dynein extracts is similar to that seen in *mia*1-1 dynein extracts (Figs. *3* and *4*). The positions of 205- and 116-kD standards are indicated.

dynein complex is phosphoregulated in a *cis/trans* asymmetric manner.

Discussion

We have identified and characterized eight mutant strains of *Chlamydomonas reinhardtii* with defects in phototactic behavior as well as defects in flagellar motility. The eight mutant strains fell into three classes that all appeared to affect the inner dynein arms. The first class consisted of the *ptm*1, *ptm*2, and *ptm*3 mutant strains. These strains had motility phenotypes that resembled the known inner dynein arm region mutant strains; they had similar swimming velocities and patterns. However, analysis of HPLC fractions did not reveal any dynein biochemical phenotypes, and these strains did not show the genetic interactions that have been indicative of inner dynein arm mutant strains. Therefore, the *ptm*$^-$ mutant strains were a new class of flagellar motility mutant strains that shared some, but not all, of the phenotypes of inner arm region mutant strains. Based on mapping of the *PTM* loci, this class defined three new loci. The *ptm*1-1 and *ptm*2-1 alleles were generated by insertional mutagenesis (Tam and Lefebvre, 1993), and cloning these genes may provide further information.

The second class consisted of *f* inner dynein arm mutations, as first identified by the *pf*9-4 allele. This mutation was allelic with previously characterized *PF*9/*IDA*1 mutations; this locus encodes a dynein heavy chain (Porter, 1996). *pf*9-4 cells displayed three phenotypes that were observed for other alleles at this locus (Kamiya et al., 1991; Kagami and Kamiya, 1992; Porter et al., 1992). The *pf*9-4 cells swam at one-half the velocity of the wild-type strain, showed additive or synthetic interactions in double mutant strains with defects in outer dynein arm or other inner dynein arm complexes, and were missing the five polypeptides of the *f* inner dynein arm complex (Fig. 2). When the phototaxis phenotypes of known dynein arm mutant strains were examined, all strains lacking the *f* inner dynein arm complex were unable to perform phototaxis. The phototaxis and motility phenotypes cosegregated with three *PF*9/*IDA*1 alleles, one *IDA*2 allele, and one *IDA*3 allele. The *f* dynein complex is unique among the outer and inner dynein arms or the drc in that mutations that remove the outer arms, the *a*, *c*, *d*, or *e* inner arm dyneins, or the drc retain the ability to perform phototaxis. It remains possible that the *b*, *g*, or as yet biochemically unresolved dynein could also play a role in phototaxis.

The third class consisted of the *mia*1-1 and *mia*2-1 strains. Cells from these strains swam at less than one-half the velocity of wild-type cells and had slightly jerky motility phenotypes; the overall motility phenotype was novel. The epistasis relationships between the *mia*$^-$ strains and mutant strains missing dynein arm region structures showed that the Mia$^-$ phenotypes were likely to require the presence of the *f* inner dynein arms (Table III). Further support of this hypothesis was provided when dynein extracts from the *mia*$^-$ strains were found to contain altered phosphorylated species of the 138-kD *f* intermediate chain based on sensitivity of the polypeptide species to treatment with CIP or calcineurin (Fig. 4). The three classes pointed to the role of inner arms in general, and the *f* inner dynein arm complex in particular, in the regulation of phototactic behavior.

138-kD Polypeptide Phosphorylation and f Dynein Activity

It seemed likely that the *mia*$^-$ mutations would affect the activity of the *f* inner dynein arm complex. To test this hypothesis, we indirectly monitored dynein activity using the sliding disintegration assay. The velocities that we obtained for wild-type axonemes are similar to Kurimoto and Kamiya (1991) using 0.1 mM ATP. We obtained values that were different for several of the mutant axonemes than had been reported previously. The difference between wild-type and *spf*1-1 sliding velocities from the values obtained by Smith and Sale (1992) and Porter et al. (1994) may be accounted for by improved buffer conditions (Kurimoto and Kamiya, 1991; Howard et al., 1994). Another difference among the assays was the difference in ATP concentration. We used 0.1 mM ATP, while the other assays were performed at 1.0 mM ATP. The *spf*1-1 background is useful as it allows us to examine the effects of the *mia* mutations in a more sensitive assay. Previous work (Kurimoto and Kamiya, 1991; Habermacher and Sale, 1997) measured the velocity of *ida*2 axonemes. Although *ida*2 and *pf*9-2 lack the *f* dynein complex biochemically, only the *pf*9-2 allele is able to suppress the central pair defect of *pf*16-2. These mutations may have subtle differences.

Using this assay, Howard et al. (1994) and Habermacher and Sale (1996) showed that phosphorylation affects the activity of the inner dynein arms. These workers identified both cAPK and type 1 protein phosphatase enzymatic activities that are involved in inner dynein arm phosphoregulation. When examined in an *spf*1-1 genetic background, which reduced the activity of outer dynein arms, the *mia*$^-$ axonemes had reduced dynein activity (Fig. 8). Treating *mia*1-1 *spf*1-1 axonemes with the kinase inhibitor HA-1004 fully restored dynein activity and shifted the mobility of the 138-kD polypeptide series to more wild-type positions on two-dimensional gels (Fig. 7). Treating *mia*2-1 *spf*1-1 axonemes with HA-1004 also shifted the mobility of the 138-kD polypeptide series to more wild-type positions (Fig. 7), but only partially restored dynein activity (Fig. 8). Therefore, we believe that the *mia*$^-$ mutations altered the phosphorylation levels of an *f* inner dynein arm intermediate chain, and these alterations affected the activity of *f* dynein.

Other dyneins may also be regulated by phosphorylation of intermediate and light chains. The 22S dynein from the outer arms of *Paramecium* is regulated by the phosphorylation of a 29-kD axonemal polypeptide (p29) in a cAMP- and Ca^{++}-sensitive fashion (Hamasaki et al., 1991; Barkalow et al., 1994). Translocation of brain microtubules by 22S dynein is significantly faster when p29 is thiophosphorylated. The intermediate (Dillman and Pfister, 1994) and light chains (Gill et al., 1994) of cytoplasmic dynein are also phosphorylated. Different phosphorylated isoforms of the intermediate chains are found in different cell types (Pfister et al., 1996). A regulatory role has not yet been ascribed to the different phosphorylated states of the intermediate or light chains of cytoplasmic dynein.

The series of 138-kD spots was shifted to more acidic pIs in two-dimensional gels of *mia*$^{-}$ axonemes; this shift suggested that at least some of the 138-kD polypeptide(s) were phosphorylated to a greater extent than normally seen. It is not clear if these more acidic spots represent novel, hyperphosphorylated forms or an increased quantity of relatively rare species that are not normally visualized in wild-type preparations. In either case, there is a correlation between the activity of the inner dynein arms and the mobility of the 138-kD polypeptide. *pf*9-2 axonemes lack *f* inner arms (Porter et al., 1992) and slid at velocities that were significantly slower than those of wild-type, *mia*1-1, or *mia*2-1 axonemes (Table IV). The *pf*9-2 axonemes serve as the base line for no *f* dynein activity. The *mia*1-1 axonemes had partial dynein activity, but the dynein activity was fully restored by HA-1004 treatment (Fig. 8). This level of dynein activity was correlated with a moderate alteration of the phosphorylation states of the 138-kD intermediate chain: native and altered electrophoretic mobilities of the 138 kD polypeptide were present in approximately equal amounts in *mia*1-1 dynein extracts (Fig. 3). The *mia*2-1 axonemes had partial inner dynein arm activity that was not fully restored by HA-1004 treatment (Fig. 8). *mia*2-1 dynein activity was correlated with the most severe alteration in the phosphorylation states of the 138-kD polypeptide: almost no 138-kD polypeptide species were seen with the wild-type electrophoretic mobility (Figs. 3 and 4). Because different levels of dynein activity were seen in the mutant axonemes, the level of phosphorylation may be proportional to activity, as has been suggested for other phosphorylation-regulated events (Soderling, 1975; Ward et al., 1986), rather than a two-state on–off model (Herskowitz, 1995; Hunter, 1995). If a proportional model is correct, we would predict that the sliding velocity of *uni*1-1 axonemes would resemble the velocity of *mia*1-1 axonemes because they have similar levels of altered 138-kD polypeptide (Figs. 3 and 9).

Regulation of f Dynein Arms and Phototaxis

In what flagellar function(s) is *f* dynein regulation involved? In the absence of the *f* inner dynein arms, an abnormal waveform is generated (Brokaw and Kamiya, 1987). This suggests that the *f* complex plays an essential role in the production of the form of the wave. The *f* inner arms also appear to be involved in signaling from the central pair microtubules, as seen by the bypass suppression of a central pair microtubule assembly defect by the *pf*9-2 allele (Porter et al., 1992). Habermacher and Sale (1997) have shown that the *f* dynein complex is needed for the increased sliding disintegration velocity after kinase inhibitor treatment of radial spoke– and outer arm–deficient axonemes. In addition to these functions, our results suggested that the *f* dynein arms played a specific role in phototactic behavior.

A cell could change its direction by differentially altering either the beat frequency or the waveform of the *cis* and *trans* flagella. Differences in flagellar beat frequency were originally postulated to play a major role in phototactic behavior. In reactivated cell models of *Chlamydomonas*, the two flagella display different beat frequencies that are reversibly controlled by Ca^{++} concentration (Kamiya and Witman, 1984). The *trans* flagellum also has an intrinsic higher beat frequency than the *cis* flagellum (Omoto and Brokaw, 1985; Kamiya and Hasegawa, 1987; Rüffer and Nultsch, 1987, 1990). Analyses of mutant strains missing outer dynein arm components show that at least part of this *cis/trans* beat frequency asymmetry requires the outer dynein arms (Sakakibara and Kamiya, 1989; Sakakibara et al., 1991). However, further analyses showed that

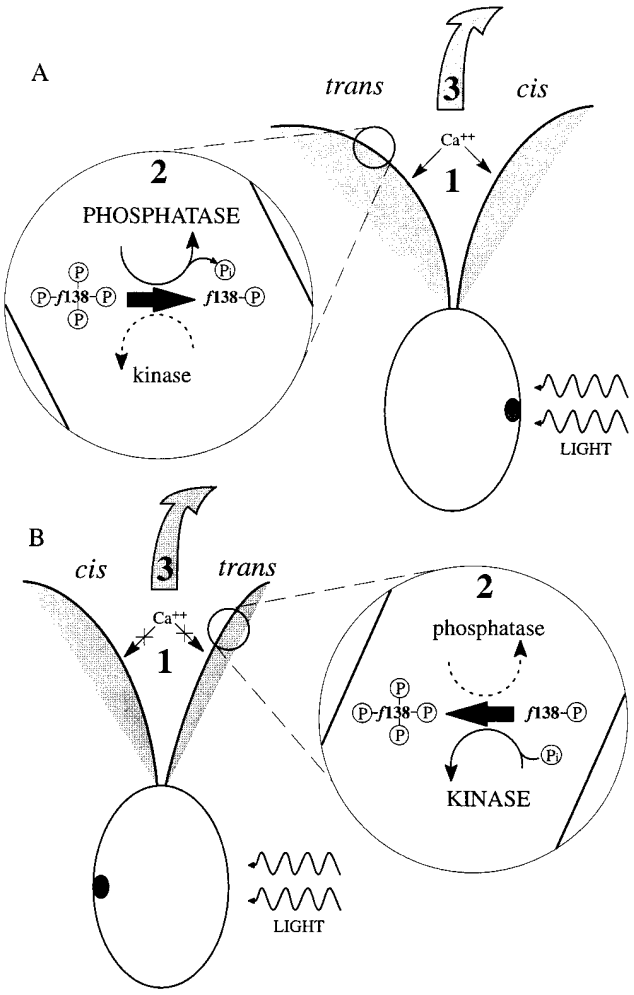

Figure 10. Schematic model of asymmetric phosphoregulation of *f* dynein activity and its role in phototaxis. When the eyespot is lighted (*A*), the rhodopsin signal is transduced to the flagellar membrane where Ca^{++} ion channels would be opened (*1*). Elevated Ca^{++} concentrations would increase the activity of the phosphatase relative to the kinase in the *trans* flagellum (*2*). This would result in the dephosphorylation of the 138-kD intermediate chain and subsequent activation of the *f* dynein complex. The *trans* flagellum would then beat with an increased front amplitude (*shaded area under flagella*) relative to the *cis* flagellum, and the cell would turn toward the light source (*3*). As the cell rotates, the eyespot becomes shaded (*B*) and the flagellar Ca^{++} ion channels would be closed (*1*). The resultant reduction in Ca^{++} ion concentration would increase the activity of the kinase relative to the phosphatase (*2*). This would lead to phosphorylation of the 138-kD intermediate chain and the deactivation of the *f* dynein complex. The *trans* flagellum would then beat with a decreased front amplitude relative to the *cis* flagellum, and the cell would continue to turn toward the light source (*3*).

the waveforms, and not the beat frequencies, of the *cis* and *trans* flagella are regulated to turn the cell (Rüffer and Nultsch, 1991).

During phototactic turning, the waveform of the *trans* flagellum has a decreased front amplitude and is less effective during the portion of the cell's rotation where the eyespot is shaded by the cell body, whereas the *cis* flagellum waveform has a decreased front amplitude and is less effective when the eyespot is unshaded (Rüffer and Nultsch, 1991). While the eyespot is shaded, less signal is postulated to be transduced to the flagellar membrane (Foster and Smyth, 1980), and there is a corresponding decrease in the activity of flagellar membrane ion channels (Hegemann et al., 1990; Harz and Hegemann, 1991). Previous results showed that Ca^{++} concentration is critical for phototactic behavior (Dolle et al., 1986; Morel-Laurens, 1987), and a Ca^{++} channel is likely located on the flagellar membrane (Harz and Hegemann, 1991).

We suggest that phosphoregulation of the *f* inner dynein arm is required for phototaxis, that the relative activity of a kinase and phosphatase is asymmetrically localized to the flagella, and that the activity of the kinase/phosphatase is mediated by Ca^{++} concentration predominantly in the *trans* flagellum. When the eyespot is in the light (Fig. 10 *A*), an elevation in Ca^{++} concentration would shift the balance of the *trans* axonemal *f* dynein phosphoregulation in favor of the phosphatase. This would result in the dephosphorylation of the 138-kD substrate, an increase in *f* dynein activity, and, ultimately, a more effective *trans* flagellar waveform. Conversely, when the eyespot is shaded (Fig. 10 *B*), the flagellar Ca^{++} concentration would decrease and the phosphoregulation would shift in favor of the kinase. This would lead to increased phosphorylation of the 138-kD substrate, decreased *f* inner dynein arm activity, and a less effective *trans* flagellar waveform. Regardless of whether the eyespot was lighted or shaded, the cell would always turn toward the light source. In this model, the activity of *f* dynein in the *cis* axoneme would not be responsive to changes in Ca^{++} concentration and would remain more or less constant throughout the rotation of the cell. It is possible that the same phosphatase studied in the in vitro experiments of Habermacher and Sale (1996) could be involved in the model, but we favor the idea of a calcineurin-like phosphatase that is activated by calcium. Tash (1989) showed that calcineurin is found in flagella of many organisms and suggested a role for calcineurin in regulating dynein activity.

Applying this model to the examined mutant strains, the loss of the entire *f* dynein complex in the *pf*9/*ida*1^{-}, *ida*2^{-}, and *ida*3^{-} strains resulted in an inability to perform phototaxis because an end effector of the phototaxis signal transduction pathway was absent. Without the presence of the *f* dynein complex, the cells were unable to alter direction in response to light stimuli. In the *mia*$^{-}$ strains, the amount of altered phosphorylated species of the 138-kD substrate was increased (Figs. 3 and 4). This increase would be predicted to result in a less effective waveform and a concurrent loss in the response to phototactic signals. The *mia*$^{-}$ mutations could act by two general mechanisms to disrupt normal *f* dynein phosphoregulation. First, the *mia*$^{-}$ mutations could shift the balance of kinase/phosphatase activity in favor of the kinase regardless of transduction signals. The phosphatase, kinase inhibitor, and substrate are just three examples of gene products whose alteration or loss of activity could result in skewing the phosphoregulation balance. Second, the mutations could affect the asymmetric localization of regulatory components between the *cis* and *trans* flagella. Little is currently known about the assembly or nature of *cis/trans* flagellar asymmetries. The *ptx*1 strain is unable to phototax. Using the in vitro cell model assay, *ptx*1 strains appear to lack the *cis/trans* flagellar asymmetry (Horst and Witman, 1993). It will be interesting to determine if the phosphorylation patterns of the 138-kD polypeptide and the sliding velocities are altered in *ptx*1 axonemes.

Support for the model comes from several lines of evidence. First, slower migrating species of the 138-kD *f* intermediate chain were seen in the dynein extract from *uni*1-1 axonemes (Fig. 9), which contained >99% *trans* axonemes. *uni*1-1 *trans* axonemes must have a higher proportion of altered phosphorylated forms of the 138-kD chain than the wild-type *cis* and *trans* axoneme population. Second, although the results of Rüffer and Nultsch (1991) show that differences in beat frequency are not directly used in phototactic behavior, the Ca^{++}-dependent preferential beating assays of Kamiya and Witman (1984) illustrate the point that *cis/trans* asymmetries exist in the flagella that are responsive to Ca^{++} concentration. Third, our results show that the altered forms of the 138-kD substrate can be dephosphorylated by the addition of purified calcineurin (Fig. 4). Calcineurin activity is known to be elevated by increased Ca^{++} concentrations in spermatazoa from a variety of species (Tash et al., 1988). Along this same line, increasing the Ca^{++} concentration is known to indirectly inhibit cAPK activity, by stimulating dephosphorylation of the type II cAPK regulatory subunit by calcineurin (Tash et al., 1986, 1988). Therefore, the cycle of *trans* flagellum activity during phototaxis may be correlated with the periodic changes in intraflagellar Ca^{++} concentration and presumed phosphatase and kinase activities.

Habermacher and Sale (1997) have also identified the phosphorylation of the 138-kD *f* intermediate chain as a regulator of dynein arm activity. These workers took a different approach to identify which inner arm complex was required to respond to a regime of kinase and phosphatase inhibitors. They tested mutant strains missing various inner arm components and found that the activity of the *f* dynein complex was correlated with the phosphorylation state of the 138-kD *f* intermediate chain. Together, these results provide the first evidence of inner dynein arm intermediate chain phosphoregulation. Our model of *f* dynein phosphoregulation uses a type 2B phosphatase (calcineurin), whereas Habermacher and Sale (1996) have described a type 1 phosphatase in the control of *f* dynein phosphoregulation. We believe that both phosphatase activities are likely to be present in the phosphoregulation pathway. In addition, the Ptx^{-} phenotypes of the *mia*1-1 and *mia*2-1 strains directly implicate the phosphorylation of the 138-kD *f* inner dynein arm intermediate chain in the transduction of phototaxis signals.

We thank M. Lamb and C. Dieckmann for generating the UV irradiation mutant strain collection, and G. Habermacher, W. Sale, S. Myster, and M. Porter for sharing published and unpublished results. In addition, we

thank T. Giddings for performing the EM analysis, and L. Ehler and A. Palombella for critical discussion of the manuscript.

This work was supported by a grant from the National Institutes of Health (NIH) (GM-32843) to S.K. Dutcher. S.J. King was supported in part by a predoctoral fellowship from NIH (5T32-GM-07135).

Received for publication 21 August 1996 and in revised form 30 October 1996.

References

Adams, G.M.W., B. Huang, G. Piperno, and D.J.L. Luck. 1981. Central-pair microtubular complex of *Chlamydomonas* flagella: polypeptide composition as revealed by analysis of mutants. *J. Cell Biol.* 91:69–76.

Barkalow, K., T. Hamasaki, and P. Satir. 1994. Regulation of 22S dynein by a 29-kD light chain. *J. Cell Biol.* 126:727–735.

Blum, H., H. Beier, and H.J. Gross. 1987. Improved silver staining of plant proteins, RNA and DNA in polyacrylamide gels. *Electrophoresis.* 8:93–97.

Brokaw, C.J., and R. Kamiya. 1987. Bending patterns of *Chlamydomonas* flagella: IV. Mutants with defects in inner and outer dynein arms indicate differences in dynein arm function. *Cell Motil.* 8:68–75.

Cohen, P. 1982. The role of protein phosphorylation in neural and hormonal control of cellular activity. *Nature (Lond.).* 296:613–620.

Debuchy, R., S. Purton, and J.-D. Rochaix. 1989. The argininosuccinate lyase gene of *Chlamydomonas reinhardtii*: an important tool for nuclear transformation and for correlating the genetic and molecular maps of the ARG7 locus. *EMBO (Eur. Mol. Biol. Organ.) J.* 8:2803–2809.

Dillman, J.F., III, and K.K. Pfister. 1994. Differential phosphorylation in vivo of cytoplasmic dynein associated with anterograde moving organelles. *J. Cell Biol.* 127:1671–1682.

Dolle, R., J. Pfau, and W. Nultsch. 1986. Role of calcium ions in motility and phototaxis of *Chlamydomonas reinhardtii. J. Plant Physiol.* 126:467–473.

Dutcher, S.K., B. Huang, and D.J.L. Luck. 1984. Genetic dissection of the central pair microtubules of the flagella of *Chlamydomonas reinhardtii. J. Cell Biol.* 98:229–236.

Dutcher, S.K., W. Gibbons, and W.B. Inwood. 1988. A genetic analysis of suppressors of the *PF10* mutation in *Chlamydomonas reinhardtii. Genetics.* 120: 965–976.

Dutcher, S.K., J. Power, R.E. Galloway, and M.E. Porter. 1991. Reappraisal of the genetic map of *Chlamydomonas reinhardtii. J. Hered.* 82:295–301.

Ehler, L.L., J.A. Holmes, and S.K. Dutcher. 1995. Loss of spatial control of the mitotic spindle apparatus in a *Chlamydomonas reinhardtii* mutant strain lacking basal bodies. *Genetics.* 141:945–960.

Fernández, E., R. Schnell, L.P. Ranum, S.C. Hussey, C.D. Silflow, and P.A. Lefebvre. 1989. Isolation and characterization of the nitrate reductase structural gene of *Chlamydomonas reinhardtii. Proc. Natl. Acad. Sci. USA.* 86: 6449–6453.

Foster, K.W., and R.D. Smyth. 1980. Light antennas in phototactic algae. *Microbiol. Rev.* 44:572–636.

Gardner, L.C., E. O'Toole, C.A. Perrone, T. Giddings, and M.E. Porter. 1994. Components of a "dynein regulatory complex" are located at the junction between the radial spokes and the dynein arms in *Chlamydomonas* flagella. *J. Cell. Biol.* 127:1311–1325.

Gill, S.R., D.W. Cleveland, and T.A. Schroer. 1994. Characterization of DLC-A and DLC-B, two families of cytoplasmic dynein light chain subunits. *Mol. Biol. Cell.* 5:645–654.

Goodenough, U.W., B. Gebhart, V. Mermall, D.R. Mitchell, and J.E. Heuser. 1987. High-pressure liquid chromatography fractionation of *Chlamydomonas* dynein extracts and characterization of inner-arm dynein subunits. *J. Mol. Biol.* 194:481–494.

Gordon, J.A. 1991. Use of vanadate as protein-phosphotyrosine phosphatase inhibitor. *Methods Enzymol.* 201:477–482.

Habermacher, G., and W.S. Sale. 1996. Regulation of flagellar dynein by an axonemal type-1 phosphatase in *Chlamydomonas. J. Cell Sci.* 109:1899–1907.

Habermacher, G., and W.S. Sale. 1997. Regulation of flagellar dynein by phosphorylation of a 138-kD inner arm dynein intermediate chain. *J. Cell Biol.* 136:167–176.

Hamasaki, T., K. Barkalow, J. Richmond, and P. Satir. 1991. cAMP-stimulated phosphorylation of an axonemal polypeptide that copurifies with the 22S dynein arm regulates microtubule translocation velocity and swimming speed in *Paramecium. Proc. Natl. Acad. Sci. USA.* 88:7918–7922.

Harris, E.H. 1989. The *Chlamydomonas* Sourcebook. Academic Press, San Diego. 780 pp.

Harz, H., and P. Hegemann. 1991. Rhodopsin-regulated calcium currents in *Chlamydomonas. Nature (Lond.).* 351:489–491.

Hasegawa, E., H. Hayashi, S. Asakura, and R. Kamiya. 1987. Stimulation of in vitro motility of *Chlamydomonas* axonemes by inhibition of cAMP-dependent phosphorylation. *Cell Motil.* 8:302–311.

Heery, D.M., F. Gannon, and R. Powell. 1990. A simple method for subcloning DNA fragments from gel slices. *Trends Genet.* 6:173.

Hegemann, P., and B. Bruck. 1989. The light-induced stop response in *Chlamydomonas reinhardtii*; occurrence and adaptation phenomena. *Cell Motil.* 14: 123–128.

Hegemann, P., K. Neumeier, U. Hegemann, and E. Kuehnle. 1990. The role of calcium in *Chlamydomonas* photomovement responses as analysed by calcium channel inhibitors. *Photochem. Photobiol.* 52:575–583.

Herskowitz, I. 1995. MAP kinase pathways in yeast: for mating and more. *Cell.* 80:187–197.

Hidaka, H., M. Inagaki, S. Kawamoto, and Y. Sasaki. 1984. Isoquiolinesulfonamides, novel and potent inhibitors of cyclic nucleotide dependent protein kinase and protein kinase C. *Biochemistry.* 23:5036–5041.

Horst, C.J., and G.B. Witman. 1993. *ptx1*, a nonphototactic mutant of *Chlamydomonas*, lacks control of flagellar dominance. *J. Cell Biol.* 120:733–741.

Howard, D.R., G. Habermacher, D.B. Glass, E.F. Smith, and W.S. Sale. 1994. Regulation of *Chlamydomonas* flagellar dynein by an axonemal protein kinase. *J. Cell Biol.* 127:1683–1692.

Huang, B., G. Piperno, and D.J.L. Luck. 1979. Paralyzed flagella mutants of *Chlamydomonas reinhardtii* defective for axonemal doublet microtubule arms. *J. Biol. Chem.* 254:3091–3099.

Huang, B., Z. Ramanis, and D.J.L. Luck. 1982*a.* Suppressor mutations in *Chlamydomonas* reveal a regulatory mechanism for flagellar function. *Cell.* 28:115–124.

Huang, B., Z. Ramanis, S.K. Dutcher, and D.J.L. Luck. 1982*b.* Uniflagellar mutants of *Chlamydomonas*: evidence for the role of basal bodies in transmission of positional information. *Cell.* 29:745–753.

Hunter, T. 1995. Protein kinases and phosphatases: the yin and yang of protein phosphorylation and signaling. *Cell.* 80:225–236.

Johnson, D.E., and S.K. Dutcher. 1991. Molecular studies of linkage group XIX of *Chlamydomonas reinhardtii*: evidence against a basal body location. *J. Cell Biol.* 113:339–346.

Kagami, O., and R. Kamiya. 1992. Translocation and rotation of microtubules caused by multiple species of *Chlamydomonas* inner-arm dynein. *J. Cell Sci.* 103:653–664.

Kamiya, R. 1988. Mutations at twelve independent loci result in absence of outer dynein arms in *Chlamydomonas reinhardtii. J. Cell Biol.* 107:2253–2258.

Kamiya, R. 1995. Exploring the function of inner and outer dynein arms with *Chlamydomonas* mutants. *Cell Motil. Cytoskeleleton.* 32:98–102.

Kamiya, R., and E. Hasegawa. 1987. Intrinsic difference in beat frequency between the two flagella of *Chlamydomonas reinhardtii. Exp. Cell Res.* 173: 299–304.

Kamiya, R., and G.B. Witman. 1984. Submicromolar levels of calcium control the balance of beating between the two flagella in demembranated models of *Chlamydomonas. J. Cell Biol.* 98:97–107.

Kamiya, R., E. Kurimoto, and E. Muto. 1991. Two types of *Chlamydomonas* flagellar mutants missing different components of inner-arm dynein. *J. Cell Biol.* 112:441–447.

King, S.J. 1996. Dynein regulation and flagellar asymmetry in *Chlamydomonas reinhardtii.* Ph.D. thesis. University of Colorado at Boulder. 168 pp.

King, S.J., W.B. Inwood, E.T. O'Toole, J. Power, and S.K. Dutcher. 1994. The *bop2-1* mutation reveals radial asymmetry in the inner dynein arm region of *Chlamydomonas reinhardtii. J. Cell Biol.* 126:1255–1266.

Kurimoto, E., and R. Kamiya. 1991. Microtubule sliding in flagellar axonemes of *Chlamydomonas* mutant mising inner- or outer-arm dynein: velocity measurement on new types of mutants by an improved method. *Cell Motil. Cytoskeleton.* 19:275–281.

Luck, D.J.L., and G. Piperno. 1989. Dynein arm mutants of *Chlamydomonas. In* Cell Movement. F.D. Warner, P. Satir, and I.R. Gibbons, editors. Alan R. Liss Inc., New York. 49–60.

Mastronarde, D.N., E.T. O'Toole, K.L. McDonald, J.R. McIntosh, and M.E. Porter. 1992. Arrangement of inner dynein arms in wild-type and mutant flagella of *Chlamydomonas. J. Cell Biol.* 118:1145–1162.

Mitchell, D.R., and J.L. Rosenbaum. 1985. A motile *Chlamydomonas* flagellar mutant that lacks outer dynein arms. *J. Cell Biol.* 100:1228–1234.

Morel-Laurens, N. 1987. Calcium control of phototactic orientation in *Chlamydomonas reinhardtii*: sign and strength of response. *Photochem. Photobiol.* 45: 119–128.

Okagaki, T., and R. Kamiya. 1986. Microtubule sliding in mutant *Chlamydomonas* axonemes devoid of outer or inner dynein arms. *J. Cell Biol.* 103:1895–1902.

Omoto, C., and C. Brokaw. 1985. Bending patterns of *Chlamydomonas* flagella. II. Calcium effects on reactivated *Chlamydomonas* flagella. *Cell Motil. 5*:53–60.

Pazour, G.J., O.A. Sineshchekov, and G.B. Witman. 1995. Mutational analysis of the phototransduction pathway of *Chlamydomonas reinhardtii. J. Cell Biol.* 131:427–440.

Pfister, K.K., M.W. Salata, J.F. Dillman III, K.T. Vaughan, R.B. Vallee, E. Torres, and R.J. Lye. 1996. Differential expression and phosphorylation of the 74 kD intermediate chains of cytoplasmic dynein in cultured neurons and glia. *J. Biol. Chem.* 126:727–735.

Piperno, G., and D.J.L. Luck. 1981. Inner arm dyneins from flagella of *Chlamydomonas reinhardtii. Cell.* 27:331–340.

Piperno, G., B. Huang, and D.J.L. Luck. 1977. Two-dimensional analysis of flagellar proteins from wild-type and paralyzed mutants of *Chlamydomonas reinhardtii. Proc. Natl. Acad. Sci. USA.* 74:1600–1604.

Piperno, G., B. Huang, Z. Ramanis, and D.J.L. Luck. 1981. Radial spokes of *Chlamydomonas* flagella: polypeptide composition and phosphorylation of stalk components. *J. Cell Biol.* 88:73–79.

Piperno, G., Z. Ramanis, E.F. Smith, and W.S. Sale. 1990. Three distinct inner

dynein arms in *Chlamydomonas* flagella. Molecular composition and location in the axoneme. *J. Cell Biol.* 110:379–389.
Piperno, G., K. Mead, and W. Shestak. 1992. The inner dynein arms I2 interact with a "dynein regulatory complex" in *Chlamydomonas* flagella. *J. Cell Biol.* 118:1455–1463.
Porter, M.E. 1996. Axonemal dyneins: assembly, organization, and regulation. *Curr. Opin. Cell Biol.* 8:10–17.
Porter, M.E., J. Power, and S.K. Dutcher. 1992. Extragenic suppressors of paralyzed flagellar mutations in *Chlamydomonas reinhardtii* identify loci that alter the inner dynein arms. *J. Cell Biol.* 118:1163–1176.
Porter, M.E., J.A. Knott, L.C. Gardner, D.R. Mitchell, and S.K. Dutcher. 1994. Mutations in the *SUP-PF-1* locus of *Chlamydomonas reinhardtii* identify a regulatory domain in the β-dynein heavy chain. *J. Cell Biol.* 126:1495–1507.
Rüffer, U., and W. Nultsch. 1987. Comparison of the beating of cis- and trans-flagella of *Chlamydomonas* cells held on micropipettes. *Cell Motil.* 7:87–93.
Rüffer, U., and W. Nultsch. 1990. Flagellar photoresponses of *Chlamydomonas* cells held on micropipettes: I. Change in flagellar beat frequency. *Cell Motil.* 15:162–167.
Rüffer, U., and W. Nultsch. 1991. Flagellar photoresponses of *Chlamydomonas* cells held on micropipettes: II. Change in flagellar beat pattern. *Cell Motil.* 18:269–278.
Sakakibara, H., and R. Kamiya. 1989. Functional recombination of outer dynein arms with outer arm-missing flagellar axonemes of a *Chlamydomonas* mutant. *J. Cell Sci.* 92:77–83.
Sakakibara, H., D.R. Mitchell, and R. Kamiya. 1991. A *Chlamydomonas* outer arm mutant missing the α heavy chain. *J. Cell Biol.* 113:615–622.
Segal, R.A., B. Huang, Z. Ramanis, and D.J.L. Luck. 1984. Mutant strains of *Chlamydomonas reinhardtii* that move backwards only. *J. Cell Biol.* 98:2026–2034.
Smith, E.F., and W.S. Sale. 1991. Microtubule binding and translocation by inner dynein arm subtype I1. *Cell Motil.* 18:258–268.
Smith, E.F., and W.S. Sale. 1992. Regulation of dynein-driven microtubule sliding by the radial spokes in flagella. *Science (Wash. DC).* 257:1557–1559.
Soderling, T.R. 1975. Regulation of glycogen synthetase. Specificity and stoichiometry of phosphorylation of the skeletal muscle enzyme by cyclic 3′:5′-AMP-dependent protein kinase. *J. Biol. Chem.* 250:5407–5412.
Tam, L.-W., and P.A. Lefebvre. 1993. Cloning of flagellar genes in *Chlamydomonas reinhardtii* by DNA insertional mutagenesis. *Genetics.* 135:375–384.
Tash, J.S. 1989. Protein phosphorylation: the second messenger signal transducer of flagellar motility. *Cell Motil.* 14:332–339.
Tash, J.S., and A.R. Means. 1983. Cyclic adenosine 3′,5′ monophosphate, calcium and protein phosphorylation in flagellar motility. *Biol. Reprod.* 28:75–104.
Tash, J.S., H. Hidaka, and A.R. Means. 1986. Axokinin phosphorylation by cAMP-dependent protein kinase is sufficient for activation of sperm flagellar motility. *J. Cell Biol.* 103:649–655.
Tash, J.S., M. Krinks, J. Patel, R.L. Means, C.B. Klee, and A.R. Means. 1988. Identification, characterization, and functional correlation of calmodulin-dependent protein phosphatase in sperm. *J. Cell Biol.* 106:1625–1633.
Ward, G.E., G.W. Moy, and V.D. Vacquier. 1986. Phosphorylation of membrane-bound guanylate cyclase of sea urchin spermatazoa. *J. Cell Biol.* 103: 95–101.
Witman, G.B., K. Carlson, J. Berliner, and J.L. Rosenbaum. 1972. *Chlamydomonas* flagella. Isolation and electrophoretic analysis of microtubules, matrix, and mastigones. *J. Cell Biol.* 54:507–539.